Available online at www.sciencedirect.com
SCIENCE DIRECT®
Comput. Methods Appl. Mech. Engrg. 193 (2004) 5503–5523
Computer methods in applied mechanics and engineering
www.elsevier.com/locate/cma

On micro–macro interface conditions for micro scale based FEM for inelastic behavior of heterogeneous materials

Damijan Markovic [a,b], Adnan Ibrahimbegovic [a,*]

[a] *Ecole Normale Supérieure de Cachan, LMT-Cachan, 61 avenue du président Wilson, Cachan Cedex 94235, France*
[b] *Naravoslovnotehniška fakulteta, Univerza v Ljubljani, Ljubljana, Slovenia*

Received 12 September 2003; received in revised form 19 December 2003; accepted 19 December 2003

Abstract

In this paper we introduce a two scale computational strategy for modeling the inelastic behavior of heterogeneous materials. We apply the FEM not only on the structural scale but also on the lower, so called micro scale, where it replaces the standard procedure, in which we define the material behavior through the constitutive relations. The special care is given to handling the interface condition between micro- and macro scales. The proposed approach is based on the localized Lagrange multiplier method and can lead to the realization of either displacement based or force based formulation. Numerical tests were done on porous and composite materials. We investigate the influence of the boundary conditions, micro scale representation window size and phase contrast on the heterogeneous material response of a single FE as well as of the whole structure.

Keywords: Micro–macro interface conditions; FEM; Inelastic behavior; Heterogeneous materials

1. Introduction

Almost all materials used in engineering sciences prove to be heterogeneous at some scale and this fact has to be considered when developing reliable models for their behavior. Conventionally in the structural mechanics we use the hierarchical approach to deal with heterogeneous materials, especially when the scales are significantly separated.

First, we investigate the material behavior at the micro scale, where we consider to understand sufficiently all the relevant phenomena, and try to find the relations between the significant macro scale

* Corresponding author. Tel.: +33 1 4740 2234; fax: +33 1 4740 2240.
E-mail address: ai@lmt.ens-cachan.fr (A. Ibrahimbegovic).

0045-7825/$ - see front matter © 2004 Elsevier B.V. All rights reserved.
doi:10.1016/j.cma.2003.12.072

quantities. These relations are then formulated in terms of a macro scale model, that can be further used for all structural calculations. The definition of the scale separation that we adopt here does not depend on the real scale at which we treat the problem and can be different for different materials or different situations.

However, there is increasing number of applications, where the assumptions of completely separated and decoupled scales are not justified. So, in this work we treat these problems, where the heterogeneities on the micro scale are too big with respect to the macro scale dimensions and where its typical length would affect the macro response of the structure, the phenomenon being usually called the *scale effect*. Consequently, the hierarchical approach has to be replaced by a strongly coupled multi-scale model, where sophisticated modeling methods are required on all the relevant scales.

In the framework of the hierarchical homogenization, there are two basic approaches for obtaining the macro scale response by knowing the mechanical constituents of a linear elastic heterogeneous medium (e.g. see [13]): *asymptotic homogenization theory* (e.g. see [33,1,34]) and *average field homogenization theory* (e.g. see [12,28,2]). The major difference between the approaches is that in the asymptotic theory we establish the effective properties, using the multi-scale perturbation theory, whereas in the average field theory the effective properties are obtained from the relations between the chosen volume averages of the quantities, like stress or strain tensors, estimated on the micro scale.

More precisely, in the average field theory we make the assumption of the existence of the *representative volume element* (RVE), which is considered both smaller enough than the macro scale characteristic volume and bigger enough than the heterogeneities on the micro scale. It is also required that the material is statistically homogeneous within the domain. On the other hand, main characteristics of the asymptotic theory are that the investigated medium is periodic and that the method is asymptotic. Then, this theory could be taken as a reference for a small ratio between the two scales. However, in spite of the differences in the basic assumptions, a remarkable equivalence between the two theories is observed, which also results in the possibility to combine them (see [13]).

Both approaches can further be extended for the non-linear analysis (e.g. see [35,8] for the asymptotic theory and [19,5,4,2] for the average field theory). Basic idea of the non-linear homogenization is to transformate the non-linear problem into several linear homogenization problems, which we are able to solve very efficiently. Nevertheless, such a transformation that would keep the efficiency of the linear problem resolutions is not trivial and is still being actively reexamined (e.g. see [11,2]).

Another inconvenience concerns the form of the macroscopic model, which has to be identified from the microstructure. If for the elastic material (both linear and non-linear) the macroscopic behavior can always be characterized through an elastic tensor of fourth order, this is no longer the case for the analysis of an inelastic material behavior, such as plasticity or damage. We can still try to use the classical plasticity and damage models (e.g. see [23,24]), where the elasticity tensor and different potentials to describe the internal variable evolution can be identified from the micro scale. The approach was adopted for instance in [19,5]. However, this hypothesis on the macro model formulation is not always justified for greater precisions and semi-analytical methods have to be applied (e.g. see [4,25]).

Due to the limits of the analytical approximations, which are based on several hypotheses, and to the constantly growing computer performances in the recent years many numerical approaches were considered. Most often the finite element method (FEM) was used for the calculation on the micro scale (e.g. see [3,10,18,17]). Nevertheless, some other numerical methods were developed for the same purpose (e.g. see [27,29,21,22]).

In many civil and mechanical engineering applications the scales are either weakly or strongly coupled and the modeling algorithm has to be adapted. If scales are separated enough and only weakly coupled, the two-level FEM procedure can be applied, called also FE^2 method (e.g. see [20,26,7]). In this approach we have a FE model for the structural scale and in each material point, i.e. numerical integration point in the FEM framework. The material response is obtained by the second level FE analysis. In this paper we

consider strongly coupled scales, where we equally utilize the FEM at both scales, yet the micro scale is not infinitely smaller but finitely smaller than the macro scale (e.g. see [16,9]).

We apply the localized Lagrangian multiplier method to couple the two scales [31,30]. In this context, the macro scale is the frame situated between different sub-domains, which can be interpreted as micro scale, because of its much finer FE representation. Thus, for each macro element, we have a choice using either a macroscopic model, obtained in the most convenient way, or a very fine FE model, which replaces the less exact constitutive relations. The present method could also be viewed as conceptually close to the multi-scale approach, where macro finite elements are enreached by some "bubble" functions, which represent the behavior at the micro scale (see [15]). In [15], however, the author has proposed a micro scale model based on the Green functions and integrable analytically, in contrast with our work, where the micro scale can be described by a very complex numerical model.

Note well that in this approach the macro FE model is not modified and none of the interface global degrees of freedom appear. Since the finer micro FE model beside its higher precision includes also much greater computational cost, it is necessary to use it only in areas, where we judge it is needed. It is indeed usually the case in applications, that there is a rather limited zone in the structure under loading, where complicated phenomena requiring a reliable micro scale explanation take place (e.g. plastification, cracking), whereas all the rest of the structure requires less sophisticated models.

In this context, where the scales are not completely separated, but are strongly coupled, we treat two basic ingredients of the model: (i) the micro scale based element size, called also the *window size*, and (ii) the type of interface for coupling the scales. According to the RVE concept (e.g. see [2]), the window size should be big enough in order to have a satisfying micro scale representation. On the other hand, the window size corresponds to the macro element size and the macro scale precision decreases for coarser meshes. There exists obviously an optimum window size, which is big enough to correctly describe the micro scale behavior and sufficiently small to give the good macro-scale field approximation.

If the window size is smaller than a RVE, the response will depend on the applied micro boundary conditions, which bears directly upon the choice of the interface formulation. For such a case, the concept of *apparent properties* was introduced in [14] and the hierarchy of bounds was established for the *effective properties* for the homogeneous boundary conditions. Thus, we ought to perform numerical tests to reestablish those bounds, similarly to the procedure in [17], but in the macro FE context. We do separate studies for hard inclusion and soft inclusion (voids) composite materials and compare the precision with respect to the different type of interface, displacement and stress based.

The outline of the paper is as follows. In the following section we introduce the chosen variational formulation concept and define the displacement and the stress based interface between the scales. To compare with the theoretical predictions, in Section 3 we carry out numerical tests with homogeneous and also non-homogeneous loading only on one micro scale based element. In Section 4 we investigate a simple structure under complex loading, discretized by the proposed micro scale based FE, and show the existence of the optimum macro element size. The conclusion are drawn in Section 5.

2. Strong coupling multi-scale methods

We consider a general class of heterogeneous structure problems submitted to an arbitrary loading and obeying non-linear physical laws resulting in phenomena like damage and plasticity. It is assumed that the scales are strongly coupled and that their evolution has to be calculated simultaneously. The FEM has shown undoubted efficiency in solid and structural analyses and we thus decide to use it on both scales. Therefore, the structure is meshed with a macro FE mesh and the microstructure representing volume similarly with a micro FE mesh (see Fig. 1).

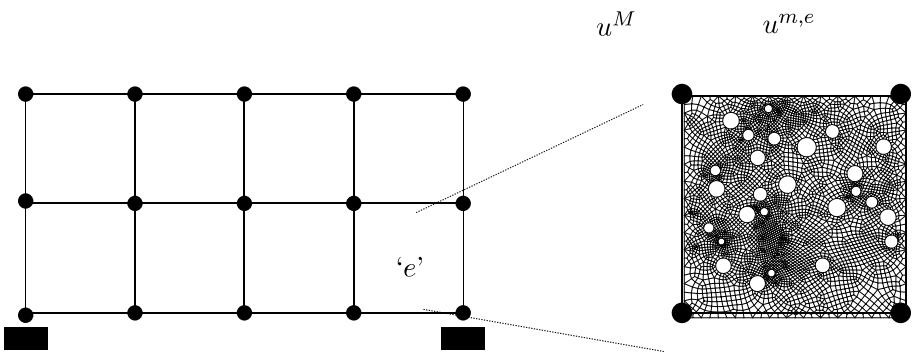

Fig. 1. Micro–macro finite element model of a simple structure. Each macro FE equally represents a meso scale window containing the microstructure information, which is again modeled by the FE mesh.

By the appropriate formulation the macro mesh element quantities (residual, stiffness etc.) are obtained from the micro FE calculation, replacing in this way the macroscopic constitutive law at the finite element level rather than at the level of a Gauss numerical integration point. It is convenient, when the macro mesh FE and the corresponding meso scale window, containing the representative microstructure details, are chosen to match perfectly. The micro–macro interface in this case is then easier to construct.

3. Micro–macro interface definition

The coupling of the scales in our multi-scale FE model is obtained through the framework of localized Lagrangian multipliers (e.g. see [31,30]). The macro mesh plays the role of a frame which is connected to the micro mesh through the Lagrangian multipliers. In the first subsection we give the general formulation and in the following we consider some particular choices for the discretization of the Lagrange multiplier space.

3.1. General formulation

We can write the elastic potential, whose stationary value will lead to the solution of the problem, as following:

$$\Pi = \Pi_{\text{micro}} + \Pi_{\text{interf}} + \Pi_{\text{ext}} \mapsto \text{stat.}, \tag{1}$$

where the different terms are defined as (Fig. 2)

$$\Pi_{\text{micro}} = \int_{\Omega^m} \Psi^m(\epsilon, \xi_k)\, \mathrm{d}V, \tag{2}$$

$$\Pi_{\text{ext}} = -\int_{\partial\Omega_\sigma} u^M t\, \mathrm{d}S - \int_{\Omega} u^m f\, \mathrm{d}V, \tag{3}$$

$$\Pi_{\text{interf}} = \int_{\Gamma} \lambda(u^m - u^M)\, \mathrm{d}S, \tag{4}$$

where u^M is macro displacement field (coarser discretization), u^m is micro displacement field (finer discretization). Accordingly, Ψ^m is micro scale free energy, ϵ is the deformation field at the micro scale, ξ_k are the

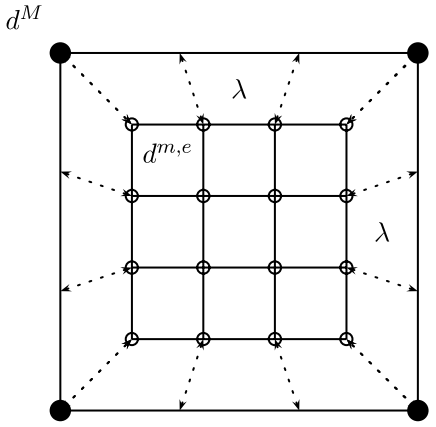

Fig. 2. Macro mesh FE connected to the micro mesh by Lagrangian multipliers λ.

internal variables at micro scale, and λ is the Lagrangian multiplier field glueing two different scales. We also note that Ω defines the total domain, $\partial\Omega_\sigma$ is the part of the boundary, where tractions are applied and Γ denotes the total interface surface between the two scales. Using the stationarity condition of the potential, $\delta\Pi = 0$, we obtain the weak formulation on the equations expressing the micro equilibrium:

$$\int_{\Omega^m} (\delta\epsilon^m \sigma^m - \delta u^m f)\,\mathrm{d}V + \int_\Gamma \delta u^m \lambda\,\mathrm{d}S = 0, \tag{5}$$

the micro–macro displacement field compatibility:

$$\int_\Gamma \delta\lambda (u^m - u^M)\,\mathrm{d}S = 0 \tag{6}$$

and the macro equilibrium:

$$\int_{\partial\Omega_\sigma} \delta u^M t\,\mathrm{d}S + \int_\Gamma \delta u^M \lambda\,\mathrm{d}S = 0. \tag{7}$$

In (5) above we use the standard kinematic and thermodynamic relation:

$$\epsilon_{ij} = \frac{1}{2}\left(\frac{\partial u_i}{\partial x_j} + \frac{\partial u_j}{\partial x_i}\right) \tag{8}$$

and

$$\sigma_{ij} = \frac{\partial \Psi(\epsilon_{kl}, \xi_k)}{\partial \epsilon_{ij}}. \tag{9}$$

Eqs. (5)–(7), completed by the set of equations determining the non-linear behavior $\sigma(\epsilon, \xi_k)$, define entirely our mechanical problem and lead to the three-field solution for u^M, λ and u^m. We discretize the fields in the framework of the FEM (e.g. see [36]) as follows:

$$u^M \approx N^M U^M, \tag{10}$$

$$\lambda \approx N^\lambda \Lambda, \tag{11}$$

$$u^m \approx N^m U^m, \tag{12}$$

which further permits us to rewrite the system (5)–(7) as

$$\begin{aligned} R_m &:= \int_{\Omega^m} (B^{mT}\sigma^m(U^m) - N^m f)\,\mathrm{d}V + \Lambda \int_\Gamma N^m N^\lambda \,\mathrm{d}S = 0, \\ R_\lambda &:= \int_\Gamma N^\lambda (N^m U^m - N^M U^M)\,\mathrm{d}S = 0, \\ R_M &:= \int_{\partial\Omega_\sigma} N^M t\,\mathrm{d}S + \Lambda \int_\Gamma N^M N^\lambda \,\mathrm{d}S = 0, \end{aligned} \tag{13}$$

where the micro and macro deformation projectors B^m and B^M are defined respectively as

$$B^m_{ijk} = \frac{1}{2}\left(\frac{\partial N^m}{\partial x_j}\delta_{ik} + \frac{\partial N^m}{\partial x_i}\delta_{jk}\right) \quad \Rightarrow \quad \hat{\epsilon}^m_{ij} = B^m_{ijk} U^m_k, \tag{14}$$

with $\hat{\epsilon}^m(U^m) = \epsilon^m|_{u^m \to N^m U^m}$ as the approximation of the strain field.

Note that the system of equation in (13) is non-linear. We choose to solve it by the Newton iterative method, which requires the linearization of the equations, such as

$$R^{(k+1)}_{(\cdot)} \approx R^{(k)}_{(\cdot)} + \frac{\partial R^{(k)}_{(\cdot)}}{\partial \eta_i}\Delta\eta_i, \tag{15}$$

where the subscript (k) denotes the value at the kth iteration and η_i the sequence of independent variables. Applying this operation, the system (13) becomes

$$\begin{pmatrix} D^{(k)} & E & 0 \\ E^{\mathrm{T}} & 0 & -F \\ 0 & -F^{\mathrm{T}} & 0 \end{pmatrix} \begin{pmatrix} \Delta U^{(k)}_m \\ \Delta\Lambda^{(k)} \\ \Delta U^{(k)}_M \end{pmatrix} = \begin{pmatrix} -R^{(k)}_m \\ -R^{(k)}_\lambda \\ -R^{(k)}_M \end{pmatrix}, \tag{16}$$

where the tensors E and F define the projection between the Lagrangian multiplier field and the micro and macro displacement field, respectively. $D^{(k)}$ denotes the value of the micro stiffness at the kth iteration. They are calculated according to:

$$E = \int_\Gamma N_m N_\lambda \,\mathrm{d}S, \tag{17}$$

$$F = \int_\Gamma N_\lambda N_M \,\mathrm{d}S, \tag{18}$$

$$D^{(k)} = \int_{\Omega^m} B^{mT} C(U^k_m) B^m \,\mathrm{d}V, \tag{19}$$

with the material stiffness tensor being

$$C_{ijkl} = \frac{\partial \sigma_{ij}}{\partial \epsilon_{kl}}. \tag{20}$$

We solve the system (16) by Gaussian elimination, eliminating first the values of ΔU^m, then $\Delta\Lambda$, ending up with a non-linear system for ΔU^M. By the elimination of variables ΔU^m and $\Delta\Lambda$ we use the operator split approach (e.g. see [16]), where for a given global–local equation problems, we first converge on the local equations with the global variables being fix and then correct the global variable approximation in order to solve the global equations.

Here, we deal with three sets of variables (U_m, Λ and U_M) and have hence three operator split iterative processes. Note, that by choosing $l_{\max} = m_{\max} = 1$ below, the procedure degenerates to the standard Gaussian elimination. In our implementation we chose to converge at each sub-loop, which leads maybe not always to the fastest algorithm but it is certainly the most robust one. So, the algorithm was implemented according to:

DO $k = 1 \ldots$ *convergence*

$$F^{\mathrm{T}} D_{\lambda}^{(k)^{-1}} F \Delta U_M^{(k)} = -\widetilde{R}_M^{(k)}$$

$$D_{\lambda}^{(k)} = E^{\mathrm{T}} D^{(k)^{-1}} E$$

$$\widetilde{R}_M^{(k)} = R_M^{(k)} + F^{\mathrm{T}} D_{\lambda}^{(k)^{-1}} R_{\lambda}^{(k)} - F^{\mathrm{T}} D_{\lambda}^{(k)^{-1}} E^{\mathrm{T}} D^{(k)^{-1}} R_m^{(k)}$$

$$\Rightarrow U_M^{(k+1)} = U_M^{(k)} + \Delta U_M^{(k)}$$

DO $l = 1 \ldots l_{\max}$ *or convergence*

$$(E^{\mathrm{T}} D^{(k,l)^{-1}} E)\ \Delta \Lambda^{(k,l)} = -\widetilde{R}_{\lambda}^{(k,l)};$$

$$\widetilde{R}_{\lambda}^{(k,l)} = -R_{\lambda}^{(k,l)} + E^{\mathrm{T}} D^{(k,l)^{-1}} R_m^{(k,l)} + F U_M^{(k)}$$

$$\Rightarrow \Lambda^{(k,l+1)} = \Lambda^{(k,l)} + \Delta \Lambda^{(k,l)}$$

DO $m = 1 \ldots m_{\max}$ *or convergence*

$$D^{(k,l,m)} \Delta U_m^{(k,l,m)} = -\widetilde{R}_m^{(k,l,m)};$$

$$\widetilde{R}_m^{(k,l,m)} = R_m^{(k,l,m)} + E \Lambda^{(k,l)}$$

$$\Rightarrow U_m^{(k,l,m+1)} = U_m^{(k,l,m)} + \Delta U_m^{(k,l,m)}$$

ENDDO m

ENDDO l

ENDDO k

Remark 1. The Gaussian elimination is not the only possibility to solve the linear system in (16). Namely, the Gaussian elimination is generally not well adapted to solving the systems with a large number of zeros on the diagonal, like our system in (16) could be, because it would lead to resolution of large and full matrices and causing thus inefficiency of the procedure. For such a sort of linear systems the iterative Uzawa algorithm is more appropriate. However, in our case the number of micro equilibrium equations exceeds largely those of the compatibility equations. Therefore, the linear system for $\Delta\Lambda$, obtained after eliminating the micro displacements, ΔU_m, will be full, but not at all big. On the other hand, elimination of the micro displacements is doable cheaply since the matrix D, obtained from the micro FE analysis and sparse, is already LU-decomposed.

Remark 2. The highest level iterative process is analogous to the iterative process of the standard non-linear FEM approach. The only difference is in the way of calculating the element residual and stiffness matrix. They are obtained through the micro FE computational process instead of a numerical integration of constitutive law. For the global (macro) process the element residual vector is calculated as $R'^{e'} = F^{\mathrm{T}}\Lambda$ and the stiffness matrix as $K'^{e'} = F^{\mathrm{T}} D_{\lambda}^{(k)^{-1}} F$.

3.2. Special case: displacement based interface

In the previous subsection we presented the variational formulation of the micro–macro interface for arbitrary interpolation functions of the three fields, u^m, λ and u^M. If the displacement interpolations, N^m and N^M, are imposed by the choice of our macro and micro FE models, for the Lagrange multiplier interpolation functions, N^{λ}, the choice is more open and can make a big difference as it will be seen in the following.

For the macro and micro FE model we applied the standard bilinear quadrilateral element technology, with the shape functions being thus:

$$N_{m,M}^{1,2,3,4}(x,y) = \tfrac{1}{4}(1 \pm x)(1 \pm y). \tag{21}$$

To get the displacement based interface, the Lagrange multiplier shape function has to have the same order of interpolation as the micro mesh boundary surface. In particular, we use the following:

$$N_{\lambda}^{i} = \Lambda_i \delta(r - r_i) \quad \forall r_i \in \partial\Omega'^{e'}, \tag{22}$$

where $\delta(\cdot)$ is the Dirac function and r_i is the coordinate vector of the ith boundary node and $\Omega'^{e'}$ denotes the macro element domain corresponding to the meso scale window.

Remark 3. Even for other possible higher order interpolations of Lagrange multipliers than that in (22), we would get the same result. Namely, in the analogy with the limitation principle of Fraeijs de Veubeke (e.g. see [6]), it is useless to increase the order of interpolation (e.g. see [36]) of the Lagrange multipliers hoping to increase accuracy more than the displacement interface condition.

By this choice we make all the displacement values at the micro mesh boundary exactly equal to the macro displacement value on the macro mesh at the same point. The result is evident by replacing (22) into the displacement compatibility equation (6), where we obtain

$$\int_{\Gamma} \delta\lambda(u^m - u^M)\,\mathrm{d}S = \delta\Lambda_i \int_{\Gamma} \delta(r - r_i)(u^m - u^M)\,\mathrm{d}S \tag{23}$$

$$\Rightarrow u^m(r_i) - u^M(r_i) = 0 \quad \forall r_i \in \partial\Omega'^{e'}. \tag{24}$$

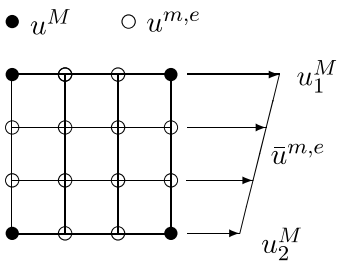

Fig. 3. Choice of the localization matrix T^e from the linear interpolation of the micro nodes displacements $\bar{u}^{m,e}$ between two adjacent macro nodes displacements $u_{1,2}^M$.

In the case when the macro shape functions, N_M, are linear on the edges, the micro mesh boundary values are obtained simply by the linear interpolation between the two adjacent macro mesh nodes (see Fig. 3):

$$u^m|_{\partial\Omega^{re}} = T^e u^M. \tag{25}$$

As expected such a displacement based interface leads to a stiffer global response (see Section 4) than the interface discussed subsequently. However, it permits to render the above presented solution algorithm more efficient. Namely, the displacement compatibility is established directly by (25) and we do not need to carry further any Lagrange multiplies, Λ_i. Hence, the three level iterative process degenerates into a two level one and also becomes much easier to implement, more robust and faster.

3.3. Special case: force based interface

In the previous subsection we choose the Lagrange multiplier shape functions such that its space dimensions equals the space dimension of the micro mesh boundary nodes. In this subsection we treat the case where the Lagrange multipliers shape functions form resembles more that of the macro displacement interpolation, i.e. linear on the edges. As we have four macro nodes per element and thus 8 degrees of freedom for a 2D case, we would have the same number of the Lagrange multiplier parameters (Fig. 4).

However, the equilibrium of forces has to be established and therefore another three conditions verified. The total number of Lagrange multiplier parameters would then be 5. More precisely, we use the optimal choice of force parameters based on the Pian–Sumihara stress interpolation (e.g. see [32]):

$$\begin{aligned} \sigma_{xx} &= \Lambda_1 + \Lambda_2 y, \\ \sigma_{yy} &= \Lambda_3 + \Lambda_4 x, \\ \sigma_{xy} &= \Lambda_5. \end{aligned} \tag{26}$$

The Pian–Sumihara element is maybe the most performant 2D quadrilateral bilinear element (e.g. see [32,36]) and the stress interpolation in (26) is considered as the optimal for the linear case. Note that the stresses are equilibrated through $\operatorname{div}\sigma = 0$. To get the values of Lagrange multipliers (forces) which ensure the displacement compatibility, we project the interpolated stresses onto the edges according to

$$\lambda(x,y) = -\sigma(x,y)\cdot n(x,y), \tag{27}$$

where n is the normal vector of the boundary surface.

In the case of force based interface the micro FE problem is defined exclusively by boundary tractions resulting from the Lagrange multiplier parametrization. Thus, we have to deal with the problem of a floating body, which is encountered most often in fluid–structure interaction problems. In our case the remedy is not overly complicated and is put in the following lines.

Let us formally decompose the displacement fields into the rigid body modes (RBM) and the deformational part:

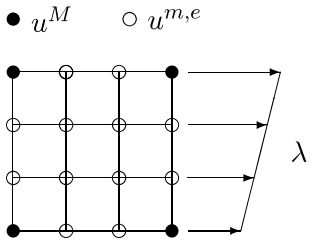

Fig. 4. In the case of the force based interface the weak displacement compatibility (Eq. (6)) is ensured through the good value of λ varying linearly on the edges.

$$u_i^m = d_i^m + R_{ij}\alpha_j^m, \tag{28}$$

$$u_i^M = d_i^M + R_{ij}\alpha_j^M, \tag{29}$$

where R is the tensor of RBM, α vector of its amplitude and d the deformational part of the displacement field. The decomposition put this way is not unique and we need the additional condition, expressing orthogonality of deformation and RBM (e.g. see [31]):

$$\int_V d_i R_{ij}\,\mathrm{d}V = 0 \tag{30}$$

to ensure the uniqueness. The decomposition is only formal and it does not affect the implementation, as it is shown in the following.

Similarly, the Lagrangian forces can in general be decomposed into the equilibrated component and the resultant component. We can use the same tensor R for the resultant forces as above for the RBM. The translations correspond to the axial forces and the rotations to the moments. So, we can write

$$\lambda_i = \chi_i + R_{ij}A_j, \tag{31}$$

with A denoting resultant amplitude and χ the equilibrated part. Note that in the interface formulation based on Pian–Sumihara stress interpolation the Lagrangian forces are already equilibrated, so that we have $\chi \equiv \lambda$ and $A \equiv 0$. In the presented approach the macro RBM are certainly well defined if the macro boundary conditions are well-posed. The micro RBM, however, should be obtained from the macro RBM through the displacement compatibility condition (6). Since λ is equilibrated by the choice of the interpolation and $\int_\Gamma \lambda_i R_{ij}\,\mathrm{d}V = 0$, (6) can be rewritten:

$$\int_\Gamma \delta\lambda(u^m - u^M)\,\mathrm{d}S = \int_\Gamma \delta\lambda(d^m - d^M)\,\mathrm{d}S = 0. \tag{32}$$

Thus, we observe that only the deformational parts d are concerned and that micro RBM, α^m can be arbitrary. In the micro FE analysis we can then fix any three independent degrees of freedom to get a well defined problem. It would be sensible to put $\alpha^m = \alpha^M$ if we wanted to recover the correct micro displacement, but since the commonly desired quantities like stress or deformation are independent of the RBM, the RBM identification is not necessary.

4. Numerical examples

In this section we compare the two proposed scale interfaces, displacement based and force based, for a microstructure representing volume smaller than commonly defined RVE. Hard inclusion composite and porous material are considered. For the sake of simplicity we took a regular microstructure (see Fig. 5) to avoid dealing with stochastic phenomena. However, we expect that the conclusions concerning the different interfaces based on results obtained with such a simplified microstructure model are valid also for a more complex microstructure model.

The second phase (hard inclusion or void) volume fraction 35% was taken the same in all calculations. The matrix behavior is modeled by the Von Mises plasticity model with the exponential hardening law. So, the yield surface is defined by

$$\Phi^p(\sigma, q^p, \xi^p) := \sqrt{\mathrm{dev}[\sigma] : \mathrm{dev}[\sigma]} - q^p(\xi^p), \tag{33}$$

where Φ^p is the yield function, ξ^p the hardening variable and $q^p(\xi^p)$ its associate stress-like quantity. The symbol dev[·] denotes the deviatoric part of the tensor,

$$\mathrm{dev}[\sigma] := \sigma - \tfrac{1}{3}\mathrm{tr}[\sigma]\mathbf{1}, \tag{34}$$

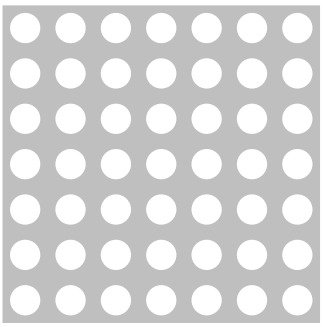

Fig. 5. Regular microstructure has been used in the study. The gray color is for the matrix and the white is for the second phase (hard inclusions or voids). The second phase volume fraction is 35% in all examples.

tr[·] denoting the trace operator and **1** the unit tensor. The exponential hardening is defined as

$$q^p(\xi^p) = \sigma_y + (\sigma_\infty - \sigma_y)(1 - \mathrm{e}^{-b\xi^p}), \tag{35}$$

where σ_y is the material yield stress, σ_∞ the saturation stress and b the exponent parameter.

We have used the following values of elasto-plastic matrix parameters:

elastic parameters (*Hooke's law*)

$$K_m = 77.9 \text{ GPa}, \tag{36}$$

$$G_m = 24.9 \text{ GPa}, \tag{37}$$

plastic parameters

$$\sigma_y = 40.0 \text{ MPa}, \tag{38}$$

$$\sigma_\infty = 80.0 \text{ MPa}, \tag{39}$$

$$b = 3000. \tag{40}$$

For the hard inclusions we assumed a linear elastic behavior with the following properties:

$$K_{\text{in}} = 545.3 \text{ GPa}, \tag{41}$$

$$G_{\text{in}} = 174.3 \text{ GPa}, \tag{42}$$

which results with $\frac{K_{\text{in}}}{K_m} = \frac{G_{\text{in}}}{G_m} = 7$.

The new micro scale based FE approach was tested in two phases. First, we did calculations on a single element containing the given microstructure and second, we analysed a microstructure with different numbers of macro elements. In Fig. 6 we show the FE mesh for the matrix and the inclusions used in our analyses.

The comparisons between the two proposed interfaces used for modeling of different materials (hard inclusion composite and porous material) by various representing volume sizes were principally based on two quantities: total external work and total plastic dissipation. The former should reflect the quality of the model from the global aspect and the latter from the local aspect, where the dissipative mechanisms, like plasticity, act. We define these quantities as

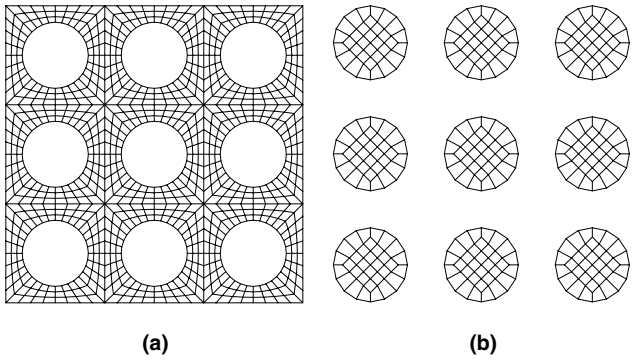

Fig. 6. FE model of the regular microstructure (Fig. 5): (a) the matrix and (b) the inclusion.

$$W_{\text{tot. ext.}} = \int_{t_1}^{t_2} \int_{\partial\Omega} F^{\text{ext}} \cdot \dot{u}\, \mathrm{d}S\, \mathrm{d}t,$$
$$\mathscr{D}_{\text{tot}} = \int_{t_1}^{t_2} \int_{\Omega} (\sigma \dot{\epsilon}^p + q^p \dot{\xi}^p)\, \mathrm{d}V\, \mathrm{d}t, \tag{43}$$

where t denotes the pseudo-time and $(\cdot)$ the corresponding derivative, F^{ext} are external boundary tractions and ϵ^p the plastic deformation. The volume integrals are calculated like in the standard FEM, the surface integral from the first equation is replaced by the sum through the boundary nodes and the pseudo-time integral is determined by the trapezoidal integration method.

4.1. Single macro-element tests

In this subsection we investigate how many heterogeneities of the given regular microstructure we have to take to have a satisfying model with respect to the total external work and the total dissipation (see the definitions in (43)) by taking the displacement or force based interface. We consider a single finite element with three different types of displacement constraints (see Fig. 7):

(i) spherical

$$u_x^2 = u_x^3 = u_y^3 = u_y^4 = u \quad \text{and} \quad u_x^1 = u_y^1 = u_y^2 = u_x^4 = 0, \tag{44}$$

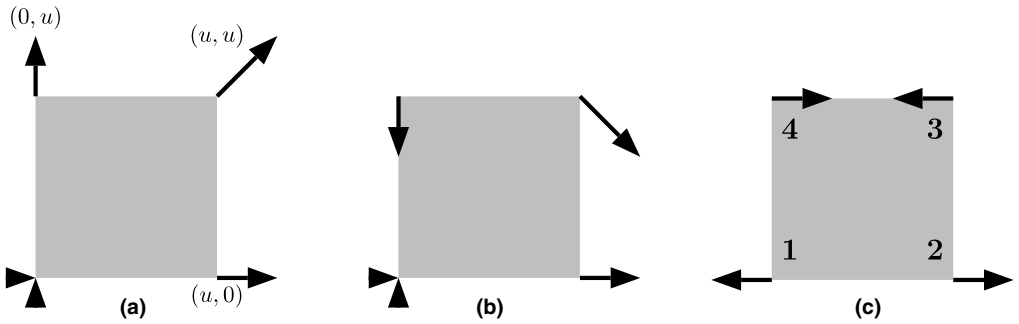

Fig. 7. The three types of boundary conditions applied to the single micro scale based finite element. The node numbering in loading definitions (44)–(46) are marked on the element on the right: (a) spherical; (b) deviatoric; (c) bending.

(ii) deviatoric

$$u_x^2 = u_x^3 = -u_y^3 = -u_y^4 = u \quad \text{and} \quad u_x^1 = u_y^1 = u_y^2 = u_x^4 = 0, \tag{45}$$

and

(iii) bending

$$-u_x^1 = u_x^2 = -u_x^3 = u_x^4 = u \quad \text{and} \quad u_y^1 = u_y^2 = u_y^3 = u_y^4 = 0, \tag{46}$$

where superscripts 1, 2, 3, 4 denote the nodes (see Fig. 7), subscripts x, y the component directions and u is a given displacement amplitude.

Note that in the case of spherical loading in 2D as shown in Fig. 7 the deviatoric component of the average deformation is not zero, since in plane strain approximation $\epsilon_{33} \equiv 0$ and thus for $\epsilon_{11} = \epsilon_{22} \neq 0$, $\operatorname{dev}\epsilon = \epsilon - \frac{1}{3}\operatorname{tr}\epsilon \neq 0$.

The spherical and deviatoric loadings are chosen because in the case of homogeneous and isotropic elastic material behavior it would completely define the mechanical response. However, our material is neither homogeneous nor elastic and we added the third, bending test. For the latter the boundary conditions are not homogeneous, that ought to be more representative of general loading to which a finite element can be submitted during structure analysis.

In Fig. 8 we show the force–displacement (F–u) diagrams, where u is the displacement amplitude of the loading and F the corresponding nodal reaction force. We considered both voids and hard inclusions as the heterogeneities of the regular microstructure (see Fig. 5) in specimen of 1×1 to 8×8 inclusions.

In Fig. 8 we observe a peculiar behavior of the hard inclusion composite under spherical loading, probably on account of the regular microstructure and the fact that the von Mises plasticity is purely deviatoric. In spite of the quasi-linear F–u behavior, the matrix plastifies, but it does not affect the global force. It turns out, that we have higher spherical stresses principally in the matrix and higher deviatoric stresses in the inclusions.

Nevertheless, in all the cases of homogeneous boundary conditions the responses are corresponding to theoretical predictions as put forward in [14]. In that paper it was established that the linear elastic stiffness obeys certain order of bounds:

$$C_s^{\text{app}}(V') \leqslant C_s^{\text{app}}(V) \leqslant C^{\text{eff}} \leqslant C_d^{\text{app}}(V) \leqslant C_d^{\text{app}}(V'); \quad V' \subseteq V, \tag{47}$$

where $C_s^{\text{app}}(V)$ denotes the apparent stiffness obtained on the volume V with homogeneous traction (stress) boundary conditions and $C_d^{\text{app}}(V)$ that with homogeneous displacement (deformation) boundary conditions. It follows thus that the apparent stiffness will give the upper bound if it is calculated using displacement boundary conditions and the lower bound when using traction boundary conditions. The values of C^{app} converge monotonously in both cases to the value of the effective stiffness, C^{eff}.

Note that the bounds in [14] were established only for linear elastic behavior, but prove here to seem to be valid also for the elasto-plastic behavior. They are however no longer valid for the bending boundary condition, which is non-homogeneous and does not respect the order of bounds in (47), at least with the respect to amplitudes, u and F. Nevertheless, the convergence of apparent stiffnesses is still present, but it is not monotonous.

The rate of convergence of the total external work (i.e. integral under the curves in Fig. 8) and the total dissipation are presented in Figs. 9 and 10, respectively. We see that both interfaces provide the convergence to the same value which reconfirms that for a big enough specimen the response does not depend on the type of the boundary conditions. On some graphs we observe small discrepancy in the converged value for the different boundary conditions, but we also have to take into account the numerical errors, which appear from the FE discretization and also from numerical integration of the two quantities, W and $\mathscr{D}$. These errors are estimated to be of the same order of magnitude as the observed discrepancies. Therefore, the approaches give the convergence to the same value within the numerical error.

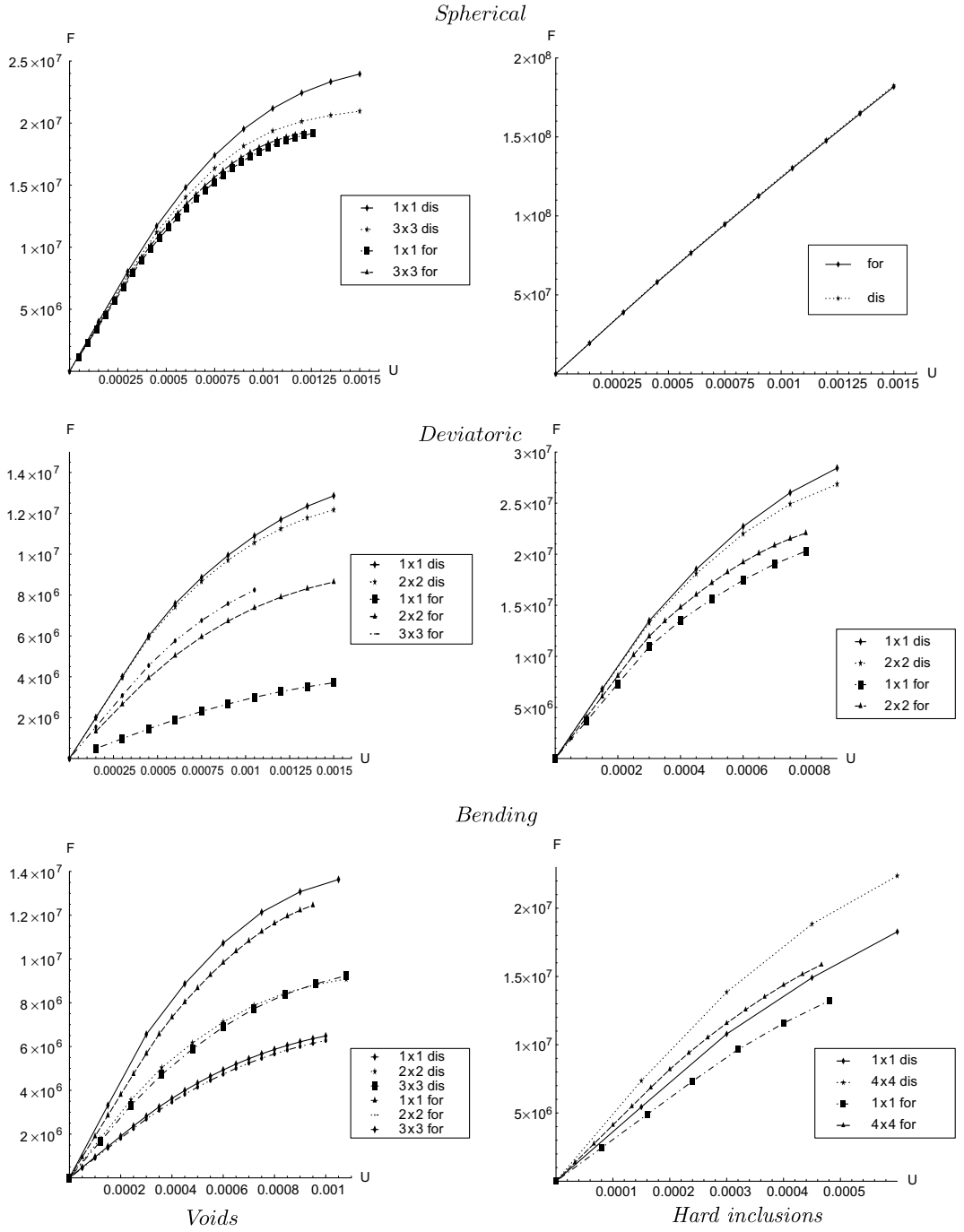

Fig. 8. $F-U$ diagrams for the material with voids (left column) and hard inclusions (right column). Three types of displacement boundary conditions were applied: spherical (above), deviatoric (in the middle) and bending (below). For each we tested both interfaces, displacement based (disp. b.i.) and force based (force b.i.) for different sizes of the meso-scale window.

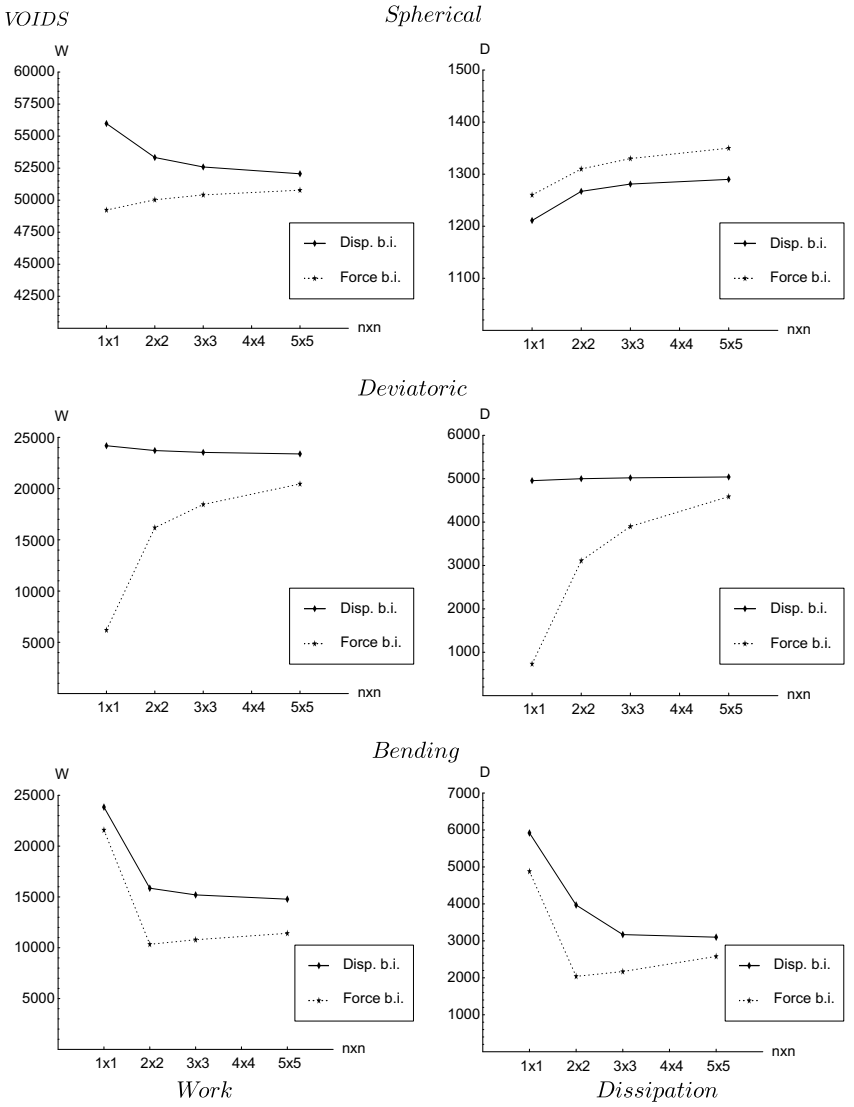

Fig. 9. Convergence rate of the total external work and the total dissipation with the increasing size of the specimen for the porous material.

Moreover, we can conclude from the diagrams that the specimen with 4×4 inclusions (voids or hard) is the smallest representative volume in respect of the total external work and the total dissipation. If the volume is smaller the quality of its representation depends on the loading it is submitted to and the type of the interface.

4.2. Micro–macro analysis example

We test the proposed FE approach on a simple heterogeneous structure, shown in the Fig. 11. The structure is completely constrained at one edge and we apply a linearly distributed displacement or traction loading on the other edge.

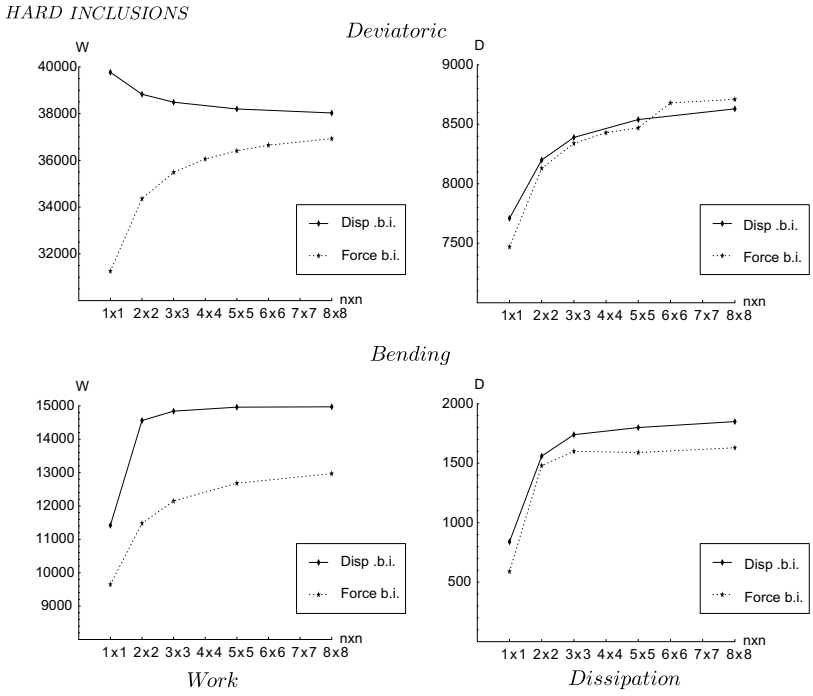

Fig. 10. Convergence rate of the total external work and the total dissipation with the increasing size of the specimen for the hard inclusion composite material.

Since the specimen is not too big, we can also use the micro FE model on the whole as the reference to compare to the results obtained by different macro FE meshes of the proposed micro–macro strategy. We calculate on the three macro meshes: 2×1, 4×2 and 8×4, which means that the meso-scale windows contain 4×4, 2×2 and 1×1 inclusions, respectively (see Fig. 12).

The results will be again given through the values of total external work and the total plastic dissipation, as in the previous subsection (see Eq. (43)). We first experiment on the porous material with the displacement amplitude of $u = 3.2 \times 10^{-4}$ or the traction amplitude of $F = 2.6 \times 10^{6}\ \mathrm{N\,m^{-2}}$. The calculations are carried out in 20 uniform increments.

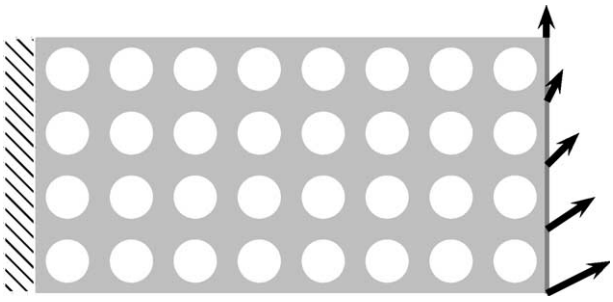

Fig. 11. Heterogeneous structure with the linearly distributed applied displacement or traction on the right edge and completely constrained at the left edge.

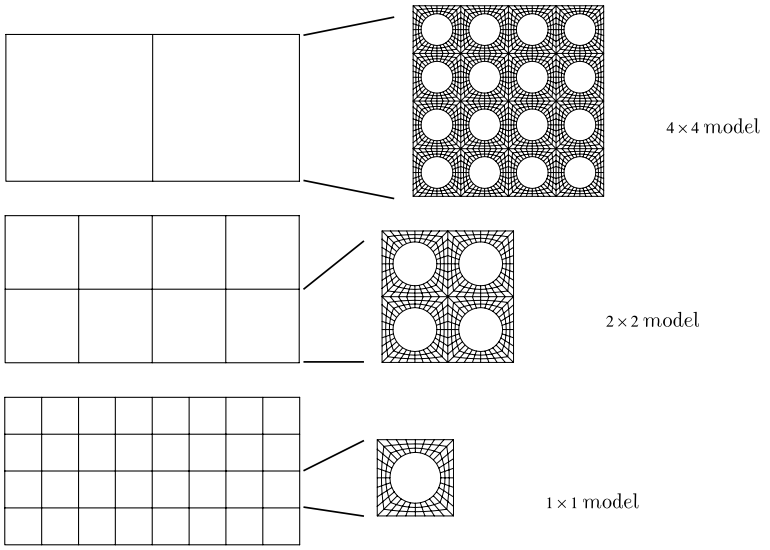

Fig. 12. Three different types of micro–macro FE models for the same heterogeneous specimen: 1×1, 2×2, 4×4.

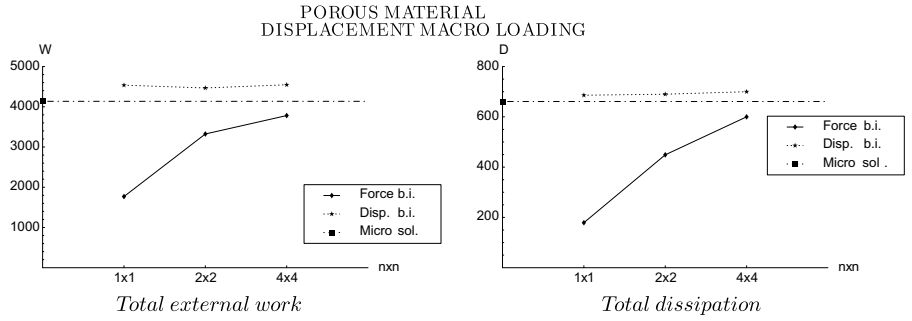

Fig. 13. Values of the total work on the left and the total dissipation on the right, (for the definitions see Eq. (43)), for different micro FE models (1×1–4×4). We compare the force based interface (force b.i.) and the displacement based interface (disp. b.i.) with the micro solution (micro sol.). For the macro b.c. the linearly distributed displacements are applied.

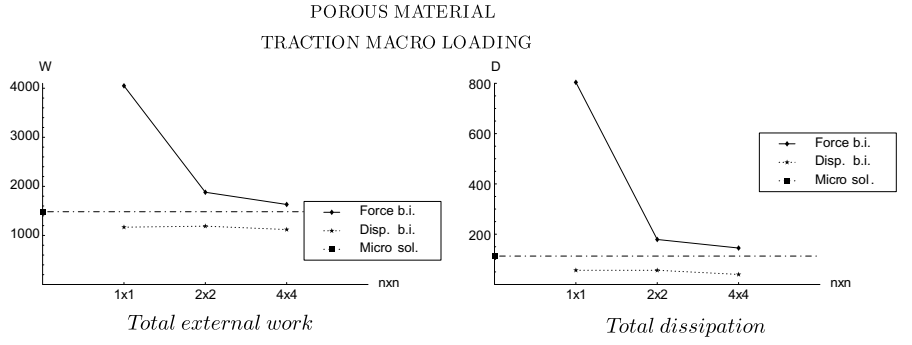

Fig. 14. Values of the total work on the left and the total dissipation on the right, (for the definitions see Eq. (43)), for different micro FE models (1×1–4×4). We compare the force based interface (force b.i.) and the displacement based interface (disp. b.i.) with the micro solution (micro sol.). For the macro b.c. the linearly distributed tractions are applied.

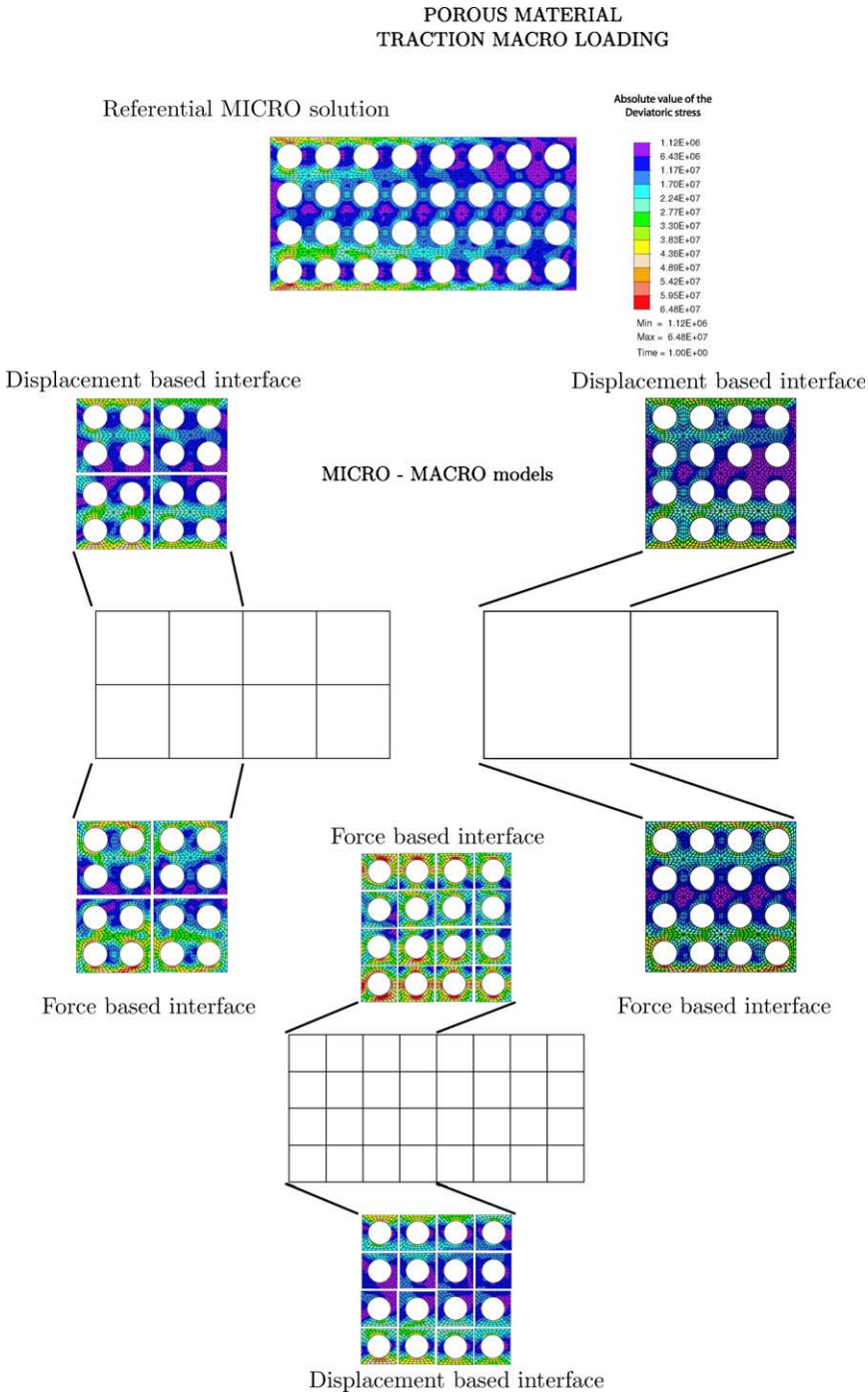

Fig. 15. Contour plots of the absolute deviatoric stresses, $\sqrt{\operatorname{dev}\sigma : \operatorname{dev}\sigma}$, of the exact micro solution and of different micro–macro models (1×1, 2×2 and 4×4). The submitted to the linearly distributed traction loading (see Fig. 11). We compare the fields obtained by using the displacement based interface or the force based interface.

The results for the global displacement loading are shown in Fig. 13 and that for the traction loading in Fig. 14. Globally, the values obtained by the proposed micro–macro strategy agree well with the reference value obtained by completely micro solution. Except for the 1×1 model with the force based interface, for which it has already been shown in the previous subsection (tests on one single macro element) that it has significantly softer behavior that the others. We also observe that the optimal macro mesh for the force based interface would be the coarsest (4×4). We can also say that it gives the most precise response of all micro–macro models. The displacement based interface, however, proves to be rather insensitive to the change of the size of the meso-scale window and seems to have a flat optimum for the 2×2 inclusions. We can also conclude that the displacement based interface gives always stiffer response that the reference micro solution and the force based interface the softer with respect to the total work and the total dissipation.

For the traction macro loading the conclusions drawn from the diagrams in Fig. 14 are similar to those for the displacement macro loading. The difference is that this time the stiffer models (displacement based interface) give smaller values for the total work, as the direct consequence of the type of the boundary conditions.

In the case of the porous material submitted to the traction loading (see Fig. 11), in addition to the work and dissipation responses (see Fig. 14), we also compare the micro–macro approaches qualitatively with

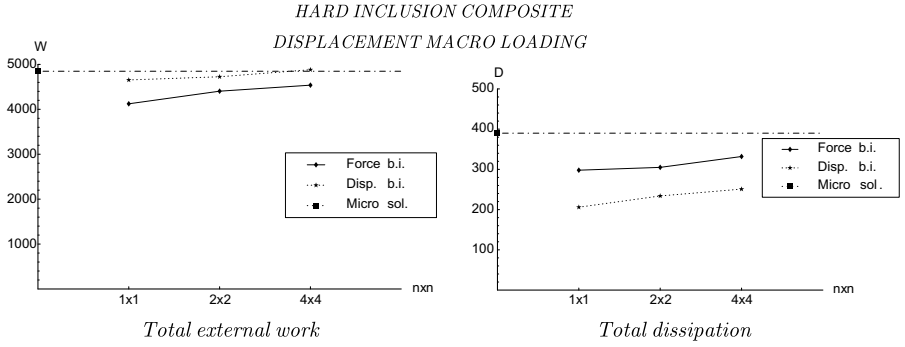

Fig. 16. Values of the total work on the left and the total dissipation on the right, (for the definitions see Eq. (43)), for different micro FE models (1×1–4×4). We compare the force based interface (force b.i.) and the displacement based interface (disp. b.i.) with the micro solution (micro sol.). For the macro b.c. the linearly distributed displacements are applied.

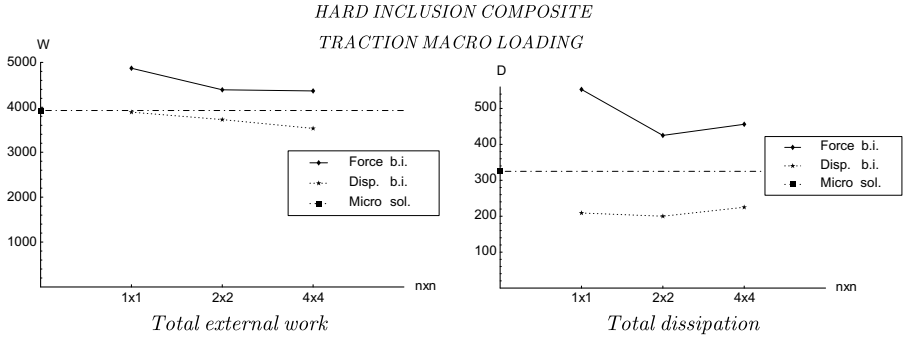

Fig. 17. Values of the total work on the left and the total dissipation on the right, (for the definitions see Eq. (43)), for different micro FE models (1×1–4×4). We compare the force based interface (force b.i.) and the displacement based interface (disp. b.i.) with the micro solution (micro sol.). For the macro b.c. the linearly distributed tractions are applied.

respect to the contours of the deviatoric part of the stress fields (see Fig. 15). It can be concluded that all the models agree on where the higher or lower deviatoric stresses will appear, albeit accentuated by different amplitudes. The amplitudes, though, seem to reconcile with the values of the total work in Fig. 14.

In the following we show the same sort of tests for the hard inclusion composite. One can conclude from Figs. 16 and 17 that quality of the results with respect to the referential micro solution is equivalent to that obtained for the porous material. The important difference is observed in that the displacement and traction based interface no longer give absolutely stiffer and softer response than the reference value (work or dissipation) as before. It is somewhat surprising that the displacement based interface gives more precise values of the work, yet the force based interface represents better the plastic dissipation.

5. Conclusion

A strong coupling micro–macro strategy was developed where the finite element method (FEM) was used both at macro- and micro scale. The micro scale is considered finitely smaller than the macro-scale, so the scales are coupled on the element level and not, as in more commonly used approach, on the integration point level. The coupling is based on the localized Lagrange multiplier procedure and does not complicate the standard macro FEM resolution. We consider two basic types of interfaces obtained by the given formulation: displacement based and force based.

The two types of interfaces were first tested numerically on a single element in order to study their influence on apparent elasto-plastic behavior. For homogeneous loading we observe a good agreement with the theoretical prediction of bounds with respect to the apparent properties, but we also observe that the bounds are no longer respected for a more general non-homogeneous loading.

In contrast to some previous results for a linear case, the force based interface does not necessarily lead to a better response in the micro–macro structural analysis with respect to the displacement based interface. We show that the choice on the interface type should depend on: the quantity(ies) we are interested in, the macro-scale loading and the micro scale window size.

Acknowledgment

This work was supported by the Slovene Ministry of Education, Science and Sport (“Mladi raziskovalec”) and the French Ministry of Research (ACI 2139).

References

[1] J.C. Michel, P. Suquet, Nonuniform transformation field analysis, Int. J. Solid Struct. 40 (2003) 6937–6955.
[2] M. Bornert, T. Bretheau, P. Gilormini, Homogénéisation en mécanique des matéteriaux, vols. I & II, Hermes-Science, Paris, 2001.
[3] J.R. Brockenbrough, S. Suresh, H.A. Wienecke, Deformation of metal-matrix composites with continuous fibers: geometrical effects of fiber distribution and shape, Acta Metall. Mater. 39 (5) (1991) 735–752.
[4] V.A. Buryachenko, F.G. Rammerstorfer, A.F. Plankensteiner, A local theory of elastoplastic deformation of two-phase metal matrix random structure composites, J. Appl. Mech. 69 (2002) 489–496.
[5] J.L. Chaboche, S. Kruch, J.F. Maire, T. Potter, Towards a micromechanics based inelastic and damage modeling of composites, Int. J. Plasticity 17 (2001) 411–439.
[6] B. Fraeijs de Veubeke, Upper and lower bounds in matrix structural analysis, AGARDograph 72 (1964) 165.
[7] F. Feyel, A multilevel finite element method (fe^2) to describe the response of highly non-linear structures using generalized continua, Comput. Methods Appl. Mech. Engrg. 192 (2003) 3233–3244.
[8] J. Fish, K. Shek, M. Pandheeradi, M.S. Shephard, Computational plasticity for composite structures based on mathematical homogenization: theory and practice, Comput. Methods Appl. Mech. Engrg. 148 (1997) 53–73.

[9] S. Ghosh, K. Lee, P. Raghavan, A multi-level computational model for multi-scale damage analysis in composite and porous materials, Int. J. Solids Struct. 38 (2001) 2335–2385.
[10] S. Ghosh, S. Moorthy, Elastic–plastic analysis of arbitrary heterogeneous materials with the voronoi cell finite element method, Comput. Methods Appl. Mech. Engrg. 121 (1995) 373–409.
[11] P. Gilormini, A shortcoming of the classical non-linear extension of the self-consistent model, C.R. Acad. Sci. Paris 320 (116) (1995) 115–122.
[12] R. Hill, Elastic properties of reinforced solids: some theoretical principles, J. Mech. Phys. Solids 11 (1963) 357–372.
[13] M. Hori, S. Nemat-Nasser, On two micromechanics theories for determining micro–macro relations in heterogeneous solids, Mech. Mat. 31 (1999) 667–682.
[14] C. Huet, Application of variational concepts to size effects in elastic heterogeneous bodies, J. Mech. Phys. Solids 38 (1990) 813–841.
[15] T.J.R. Hughes, Multiscale phenomena: Green's functions, the Dirichlet-to-Neumann formulation, subgrid scale models, bubbles and the origins of stabilized methods, Comput. Methods Appl. Mech. Engrg. 127 (1995) 387–401.
[16] A. Ibrahimbegovic, D. Markovic, Strong coupling methods in multiphase and multiscale modeling of inelastic behavior of heterogeneous structures, Comput. Methods Appl. Mech. Engrg. 192 (2003) 3089–3107.
[17] M. Jiang, I. Jasiuk, M. Ostoja-Starzewski, Apparent elastic and elastoplastic behavior of periodic composites, Int. J. Solids Struct. 39 (2002) 199–212.
[18] M. Jiang, M. Ostoja-Starzewski, I. Jasiuk, Scale-dependent bounds on effective elastoplastic response of random composites, J. Mech. Phys. Solids 49 (2001) 655–673.
[19] J.W. Ju, L.Z. Sun, Effective elastoplastic behavior of metal matrix composites containing randomly located aligned spheroidal inhomogeneities. Part i: micromechanics-based formulation, Int. J. Solids Struct. 38 (2001) 183–201.
[20] S. Kruch, J.L. Chaboche, F. Feyel, F.X. Roux, Two-scale damage analysis of components reinforced with composite materials, in: 4th World Conference on Computational Mechanics, Buenos Aires, 1998.
[21] P. Ladevè ze, O. Loiseau, D. Dureisseix, A micro–macro and parallel computational strategy for highly heterogeneous structures, Int. J. Numer. Methods Engrg. 52 (2001) 121–138.
[22] P. Ladevè ze, A. Nouy, On a multiscale computational strategy with time and space homogenization for structural mechanics, Comput. Methods Appl. Mech. Engrg. 192 (2003) 3061–3087.
[23] J. Lemaître, J.L. Chaboche, Mécanique des Matériaux Bolides, Dunod, Paris, 1988.
[24] J. Lubliner, Plasticity Theory, MacMillan, New York, 1990.
[25] J.C. Michel, P. Suquet, Nonuniform transformation field analysis, Int. J. Solids Struct, (special issue), in press.
[26] C. Miehe, Strain-driven homogenization of inelastic microstructures and composites based on an incremental variational formulation, Int. J. Numer. Methods Engrg. 55 (2002) 1285–1322.
[27] H. Moulinec, P. Suquet, A numerical method for computing the overall response of nonlinear composites with complex microstructure, Comput. Methods Appl. Mech. Engrg. 157 (1998) 69–94.
[28] T. Mura, Micromechanics of Defects in Solids, Martinus Nijhoff, New York, 1987.
[29] M. Paley, J. Aboudi, Micromechanical analysis of composites by the generalized cells model, Mech. Mater. 14 (1992) 127.
[30] K.C. Park, C.A. Felippa, A variational principle for the formulation of partitioned structural systems, Int. J. Numer. Methods Engrg. 47 (2000) 395–418.
[31] K.C. Park, C.A. Felippa, G. Rebel, A simple algorithm for localized construction of non-matching structural interfaces, Int. J. Numer. Methods Engrg. 53 (2002) 2117–2142.
[32] T.H.H. Pian, K. Sumihara, Rational approach for assumed stress finite elements, Int. J. Numer. Methods Engrg. 20 (1984) 1638–1685.
[33] E. Sanchez-Palencia, Comportement local et macroscopique d'un type de milieux physique heterogenes, Int. J. Engrg. Sci. 12 (1974) 251–331.
[34] E. Sanchez-Palencia, Non Homogeneous Media and Vibration TheoryLecture Notes in Physics, vol. 127, Springer, Berlin, 1980.
[35] P. Suquet, Local and global aspects in the mathematical theory of plasticity, in: A. Sawczuk, G. Bianchi (Eds.), Plasticity Today—Modeling Methods and Applications, Elsevier, London, 1997.
[36] O.C. Zienkiewicz, R.L. Taylor, The Finite Element Method, vols. I, II & III, Butterworth Heineman, Oxford, 2000.